Unexpected chain of redox events in Co-based Prussian Blue analogs

Polina A. Morozova[a], Sergey V. Ryazantsev[a], Artem D. Dembitskiy[a], Anatolii V. Morozov[a], Gangadhar Das[b], Giuliana Aquilanti[b], Mattia Gaboardi[b,c,d], Jasper R. Plaisier[b], Alexander A. Tsirlin[e], Igor A. Presniakov[f], Artem M. Abakumov[a], Stanislav S. Fedotov[a,*]*

[a] *Center for Energy Science and Technology, Skolkovo Institute of Science and Technology, Moscow, Russia, 143026*

[b] *Elettra - Sincrotrone Trieste S.C.p.A., Basovizza, Trieste, Italy, 34149*

[c] *Materials Physics Center, CSIC-UPV/EHU, Paseo Manuel de Lardizabal 5, Donostia - San Sebastian, Spain, 20018*

[d] *Chemistry Department, University of Pavia and C.S.G.I., Viale Taramelli, 16, Pavia, Italy, 27100*

[e] *Experimental Physics VI, Center for Electronic Correlations and Magnetism, Augsburg University, Augsburg, Germany, 86159*

[f] *Department of Chemistry, Lomonosov Moscow State University, Moscow, Russia, 119991*

**Corresponding author, email polina.morozova@skoltech.ru, s.fedotov@skoltech.ru*

Supporting Info

Table S1. Unit cell parameters of pristine powders of $K_{2-\delta}Mn_{1-x}Co_x[Fe(CN)_6]$ (x=0; 0.05; 0.10; 0.20; 0.30; 0.50; 0.60; 0.70; 0.90; 1)

x	*a*, Å	*b*, Å	*c*, Å	*β*, °	*V*, Å^3	R_p	wR_p	*GOF*
0	10.1401(5)	7.3054(3)	7.0281(3)	90.401(4)	520.61(4)	0.61	0.77	1.01
0.05	10.1409(4)	7.2966(3)	7.0401(3)	90.405(3)	520.93(3)	0.63	0.80	1.07
0.1	10.1418(3)	7.2924(2)	7.0448(3)	90.432(2)	521.02(3)	0.62	0.78	1.10
0.2	10.1454(3)	7.2688(3)	7.0584(3)	90.427(3)	520.51(3)	0.64	0.81	0.97
0.3	10.1425(4)	7.2692(3)	7.0522(2)	90.422(3)	519.94(3)	0.67	0.85	1.03
0.5	10.1309(4)	7.2669(3)	7.0445(2)	90.488(2)	518.60(1)	0.71	0.90	1.01
0.6	10.1192(3)	10.1192(3)	10.1192(3)	90	1036.18(3)	1.05	1.45	0.62
0.7	10.1059(3)	10.1059(3)	10.1059(3)	90	1032.11(3)	1.17	1.72	1.82
0.9	10.0969(2)	10.0969(2)	10.0969(2)	90	1029.35(2)	1.02	1.37	1.29

1	10.0398(1)	10.0398(1)	10.0398(1)	90	1011.99(1)	1.16	1.54	1.38

For TEM-EDX analysis the atomic fractions are described by following formulas:

$n[K] = K_{\text{atomic fraction (\%)}}/(Mn_{\text{atomic fraction (\%)}}+Co_{\text{atomic fraction (\%)}})$

$n[Mn] = Mn_{\text{atomic fraction (\%)}}/(Mn_{\text{atomic fraction (\%)}}+Co_{\text{atomic fraction (\%)}})$

$n[Co] = Co_{\text{atomic fraction (\%)}}/(Mn_{\text{atomic fraction (\%)}}+Co_{\text{atomic fraction (\%)}})$

$n[Fe] = Fe_{\text{atomic fraction (\%)}}/(Mn_{\text{atomic fraction (\%)}}+Co_{\text{atomic fraction (\%)}})$

$n[Mn]+n[Co]=1$

$n[(CN)_6]=n[Fe]=n[Fe(CN)_6]$

Table S2. Elemental composition of the series of samples $K_{2-\delta}Mn_{1-x}Co_x[Fe(CN)_6]$ calculated from STEM-EDX data

x	K	K error	Mn	Mn error	Co	Co error	Fe	Fe error
0	1.60846	0.15099	1	0.09525	0	--	0.91596	0.09525
0.05	1.45982	0.16088	0.95932	0.1623	0.04068	0.00876	0.91295	0.15948
0.1	1.58343	0.1487	0.90416	0.08633	0.09584	0.01312	0.90172	0.08609
0.2	1.45437	0.1405	0.80174	0.07959	0.19826	0.0242	0.89395	0.08753
0.3	1.30719	0.13532	0.71427	0.11928	0.28573	0.04769	0.87334	0.14589
0.5	1.37545	0.13394	0.5151	0.08433	0.4849	0.08478	0.8722	0.14166
0.6	1.2263	0.12746	0.41386	0.06974	0.58614	0.09867	0.85363	0.14255
0.7	1.19183	0.12544	0.3198	0.05453	0.6802	0.11401	0.87232	0.14568
0.9	0.83944	0.11543	0.12013	0.02273	0.87913	0.15981	0.88101	0.16514
1	0.90469	0.12134	0	--	1	0.18145	0.88991	0.16252

Table S3. Hyperfine parameters of the ^{57}Fe Mössbauer spectra for the $K_{2-\delta}Mn_{1-x}Co_x[Fe(CN)_6]$ recorded at RT

Composition (x)	δ, mm/s	Δ, mm/s	W, mm/s
0	-0.099 ± 0.001	0.078 ± 0.003	0.234 ± 0.003
0.2	-0.099 ± 0.001	0.091 ± 0.003	0.257 ± 0.003
0.5	-0.097 ± 0.001	0.113 ± 0.003	0.278 ± 0.003
0.7	-0.096 ± 0.001	0.107 ± 0.003	0.289 ± 0.003

1.0	-0.093 ± 0.001	0.071 ±0.003	0.257 ± 0.003

δ is an isomer shift, Δ is a quadrupole splitting, W is a halfwidth

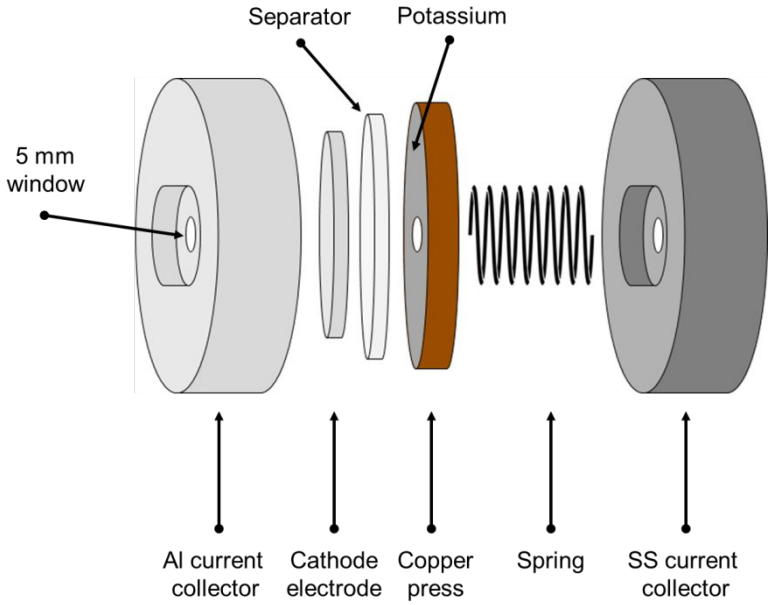

Figure S1. The principal scheme of operando cells.

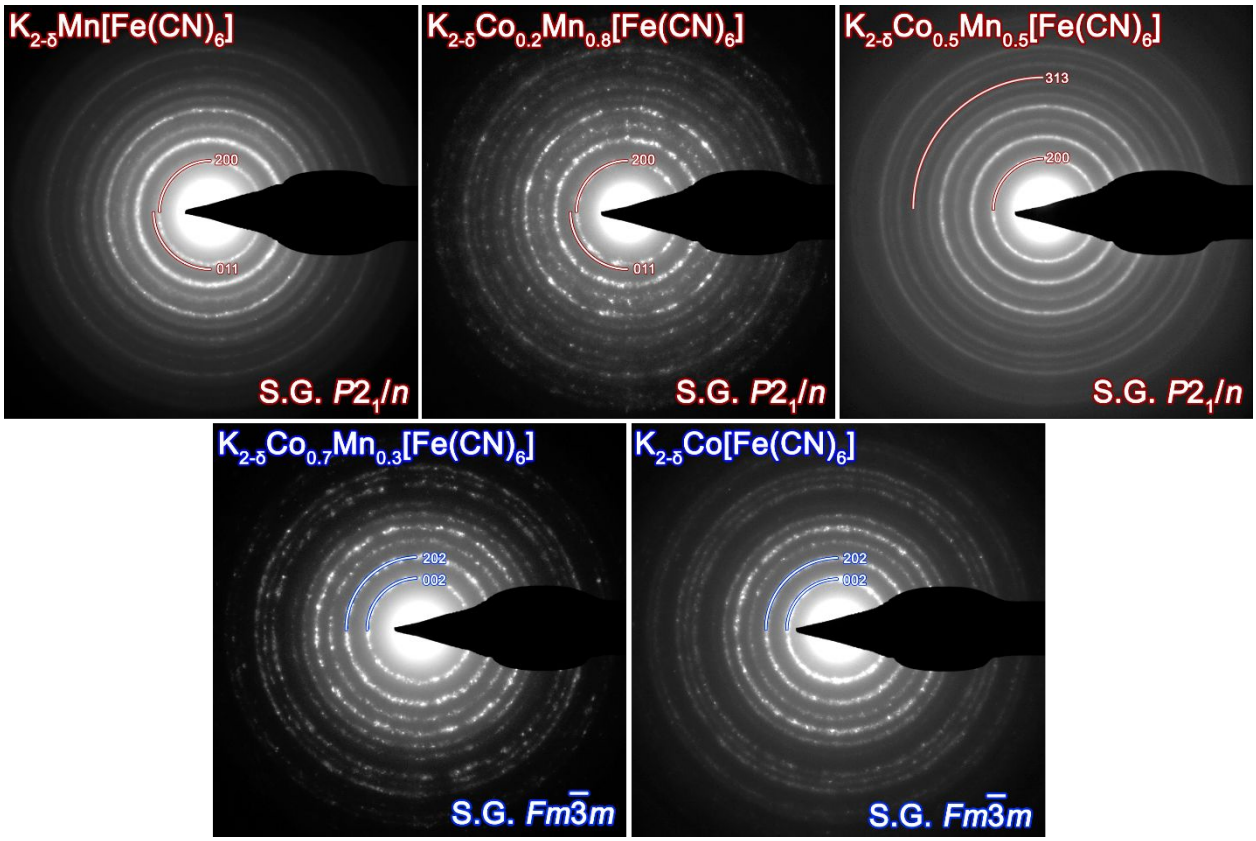

Figure S2. Ring SAED patterns of $K_{2-\delta}Mn_{1-x}Co_x[Fe(CN)_6]$ (x = 0. 0.2, 0.5, 0.7, 1.0). When Co content in $K_{2-\delta}Mn_{1-x}Co_x[Fe(CN)_6]$ is no more than 50 at. %, SAED pattern can be only indexed in monoclinic structure (S.G. $P2_1/n$),

otherwise compound crystallizes in cubic structure (S.G. $Fm\bar{3}m$) according to ring SAED. First two rings are indexed in corresponding space groups for better visual clarity.

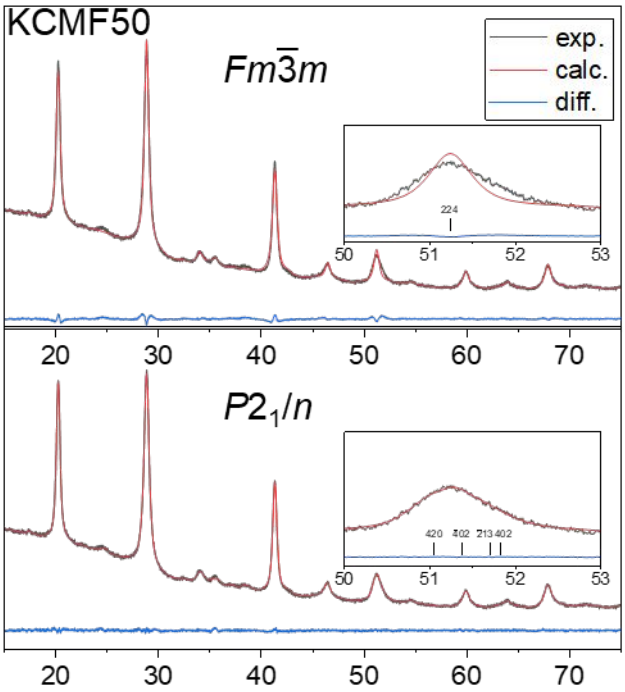

Figure S3. Le Bail profiles in $Fm3m$ (a=10.1199(2) Å, GOF=1.82, Rp=1.15, wRp=1.63) and $P2_1/n$ (a=10.1191(4) Å, b=7.2633(3) Å, c=7.0490(4) Å, β=90.488(2)˚GOF=1.00, Rp=0.70, wRp=0.89) space groups for KCMF50

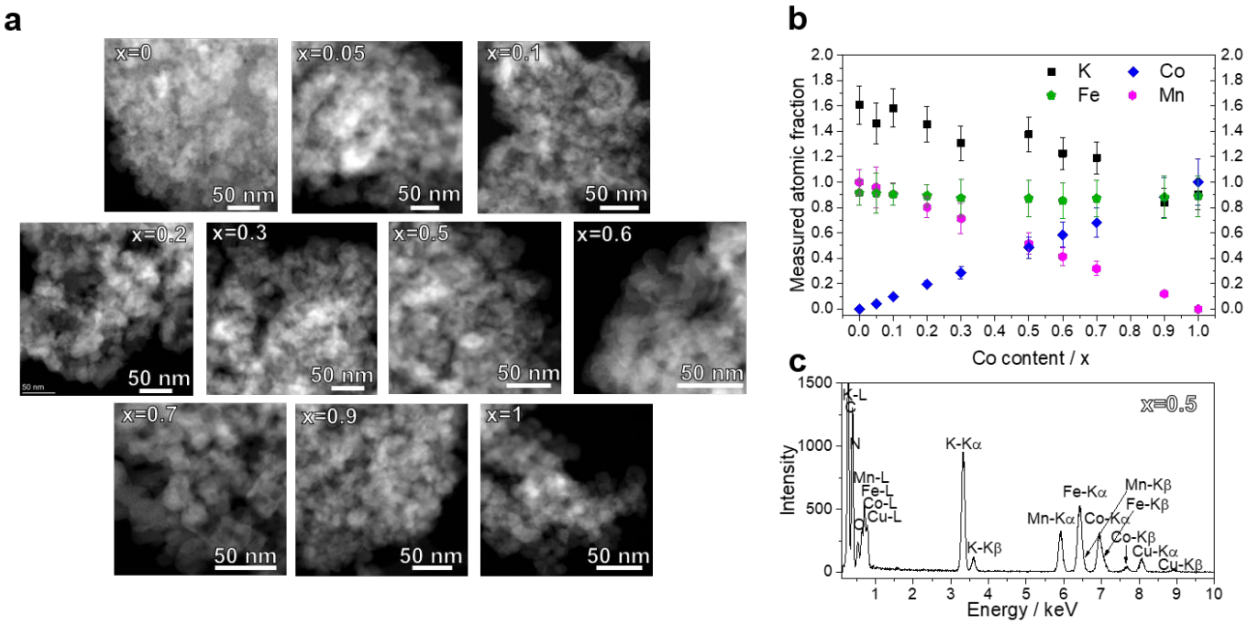

Figure S4. (a) TEM-EDX (HAADF STEM) images of $K_{2-\delta}Mn_{1-x}Co_x[Fe(CN)_6]$ (x=0; 0.05; 0.10; 0.20; 0.30; 0.50; 0.60; 0.70; 0.90; 1) nanoparticles, (b) measured atomic fraction of K, Mn, Co and Fe depending on cobalt content x plot, (c) EDX spectrum of $K_{2-\delta}Mn_{0.5}Co_{0.5}[Fe(CN)_6]$ composition

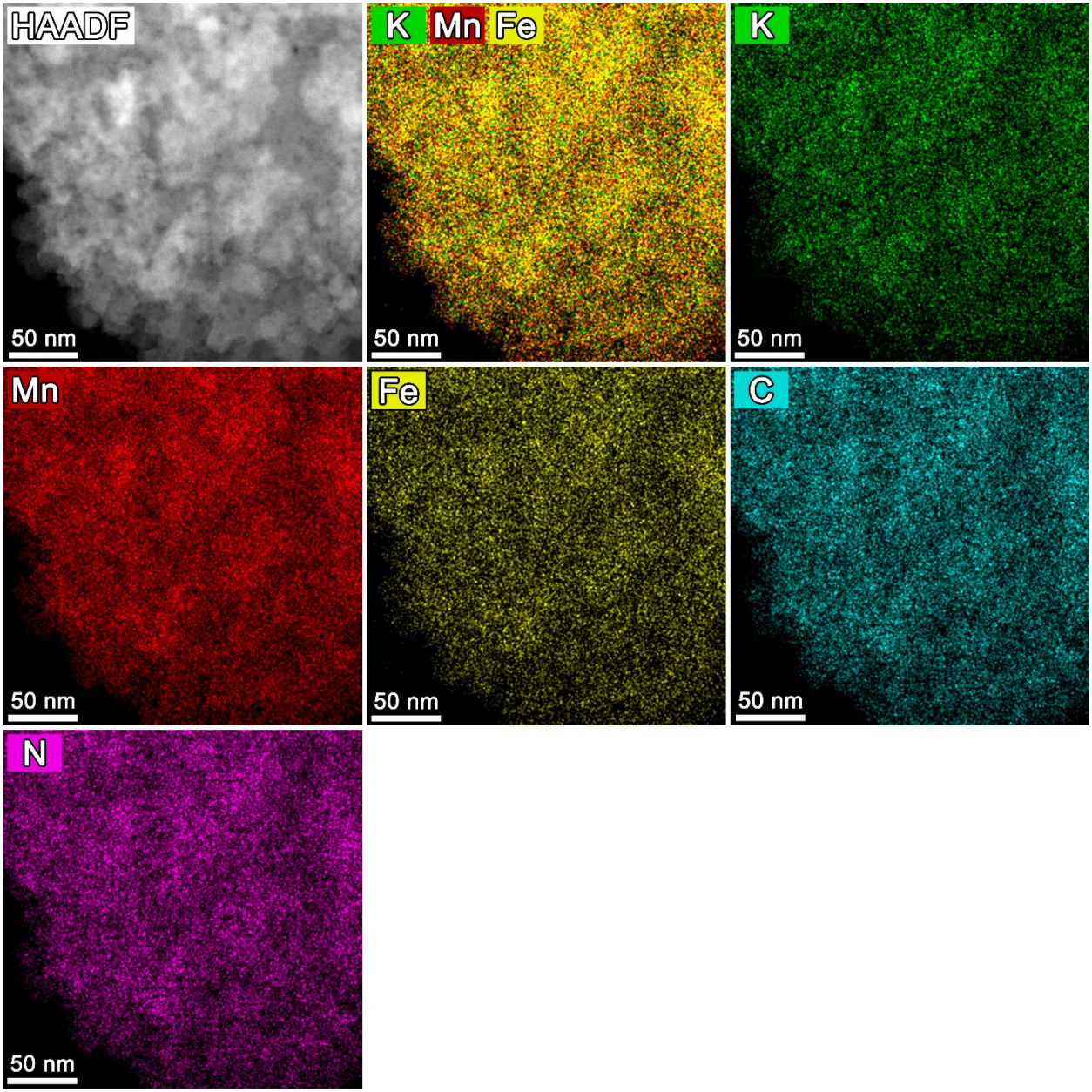

Figure S5. HAADF-STEM image of KMF along with the corresponding color-coded compositional map, elemental maps of K, Mn, Fe, C, and N.

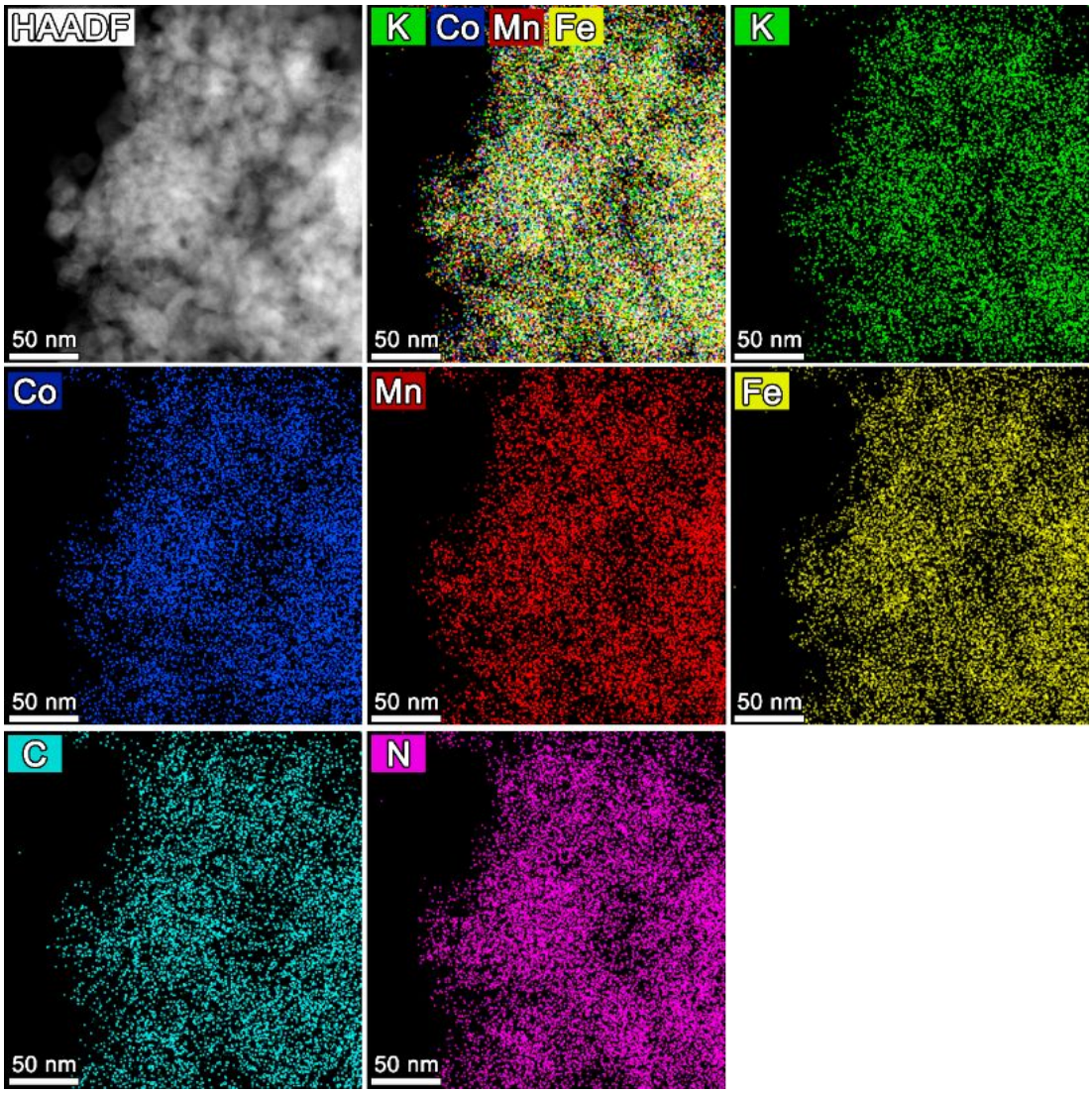

Figure S6. HAADF-STEM image of KCMF50 along with the corresponding color-coded compositional map, elemental maps of K, Co, Mn, Fe, C, and N.

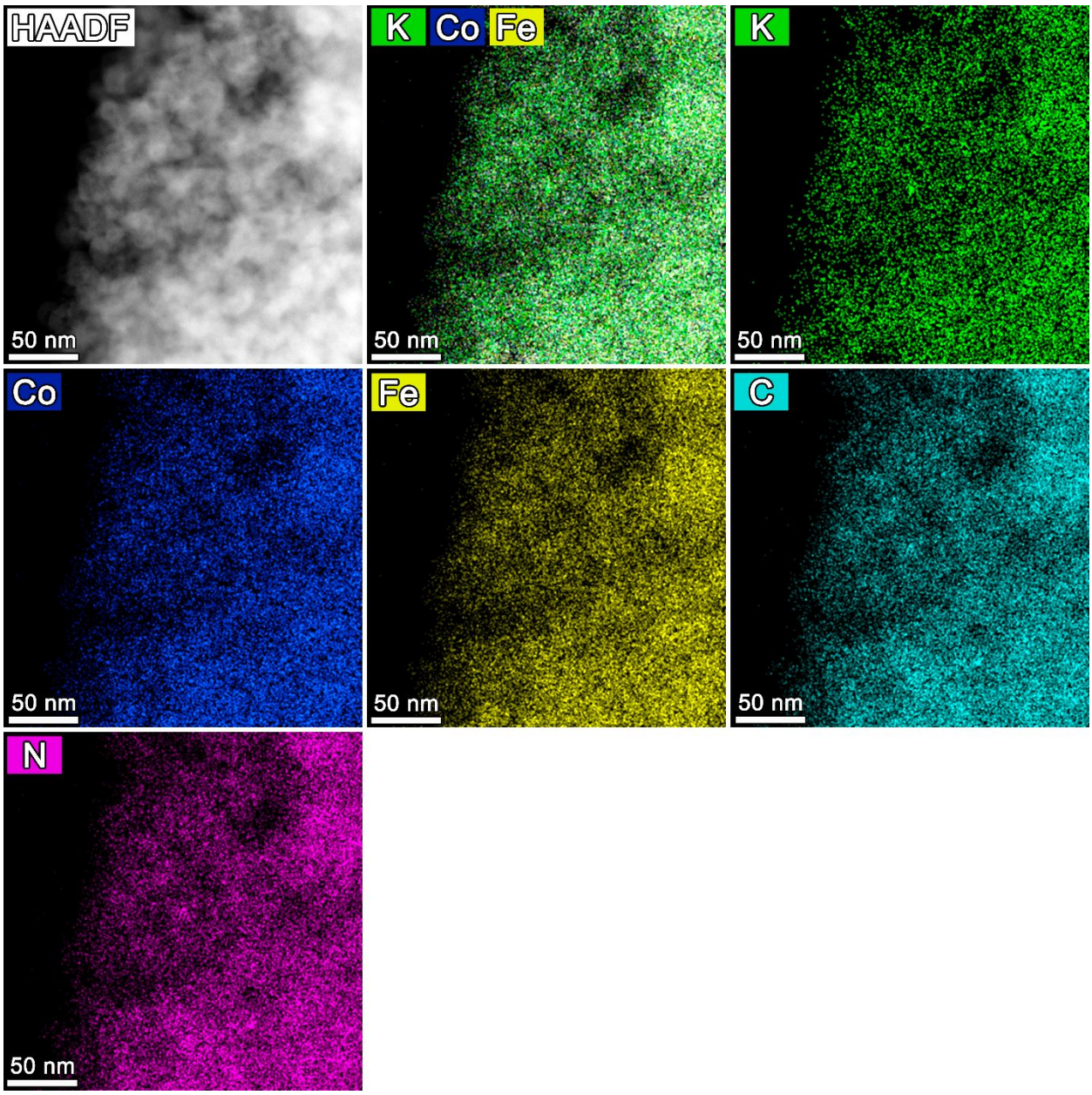

Figure S7. HAADF-STEM image of KCF along with the corresponding color-coded compositional map, elemental maps of K, Co, Fe, C, and N.

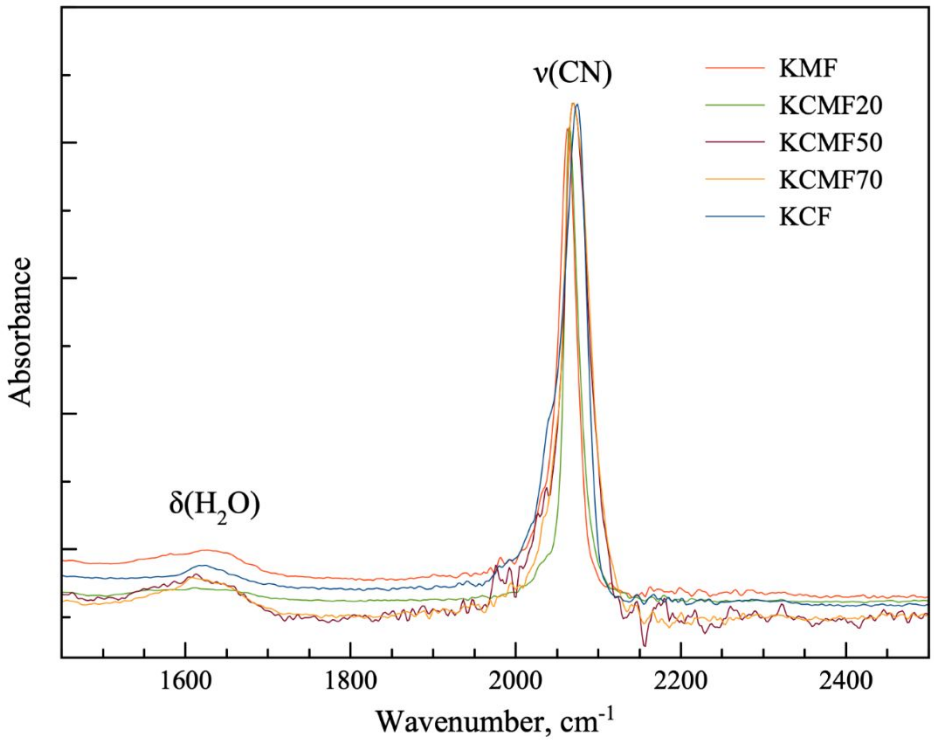

Figure S8. Fragments of the ATR-FTIR spectra (scaled for better representation) of the synthesized KCMFX materials.

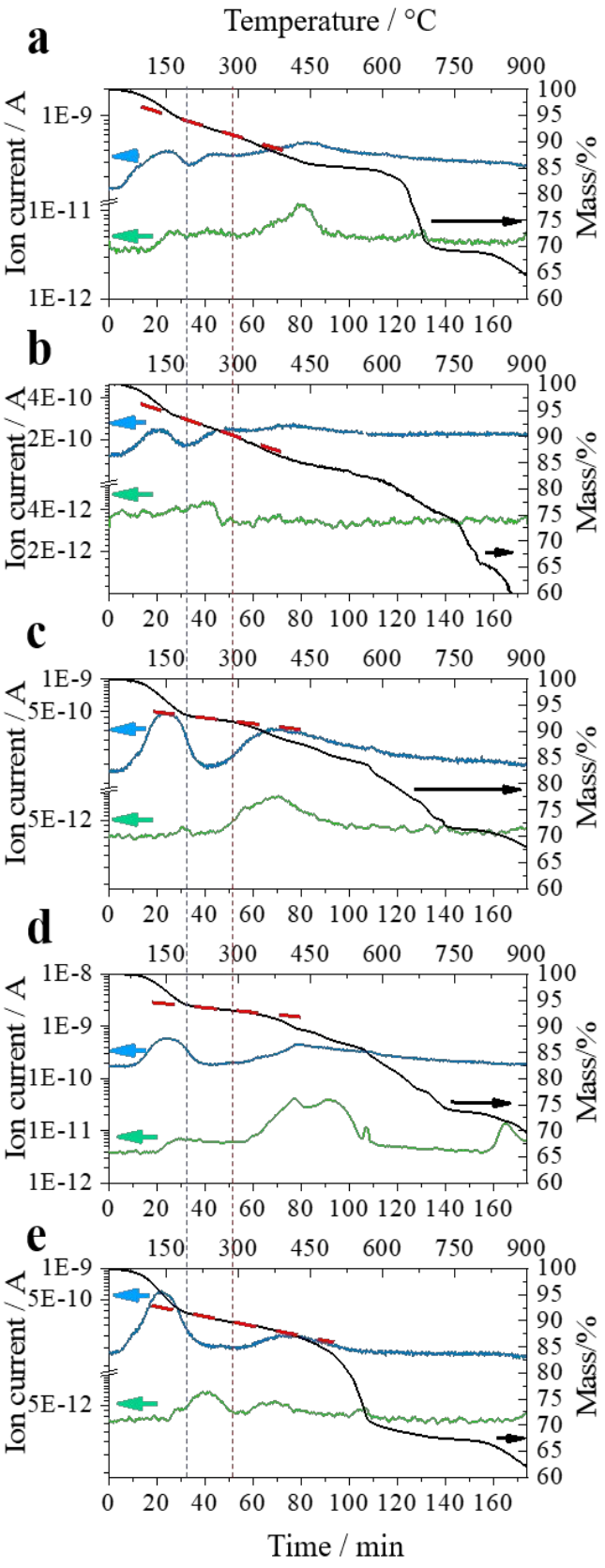

Figure S9. TGA patterns of (a) KMF, (b) KCMF10, (c) KCMF50, (d) KCMF60, and (e) KCF. Blue line is the signal from the m/z=18 ion current, corresponding to H_2O^+ ion, green line highlights the signal from the m/z=27 ion current related to HCN^+.

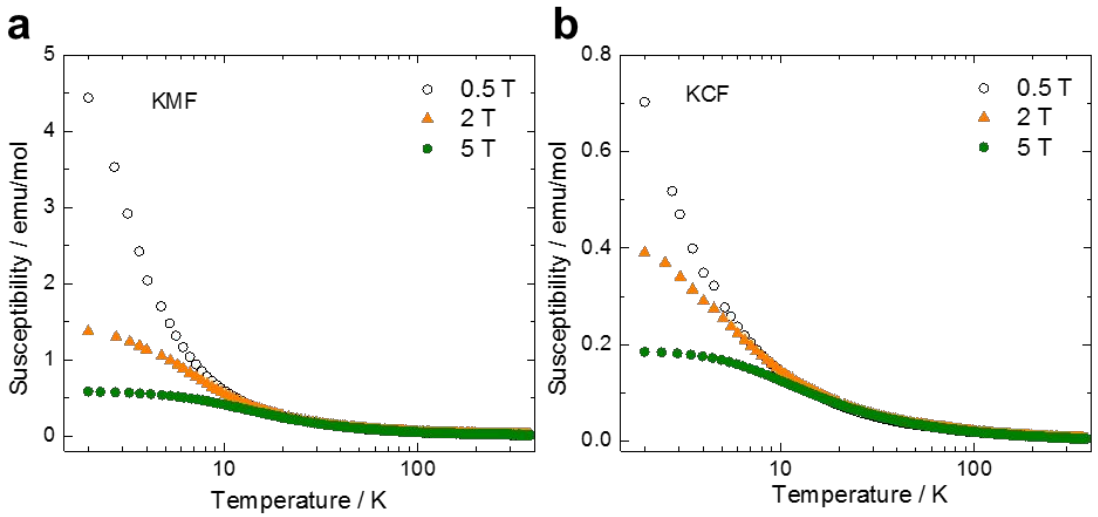

Figure S10. Magnetic susceptibility of (a) KMF and (b) KCF measured in the applied fields of 0.5 T, 2 T, and 5 T.

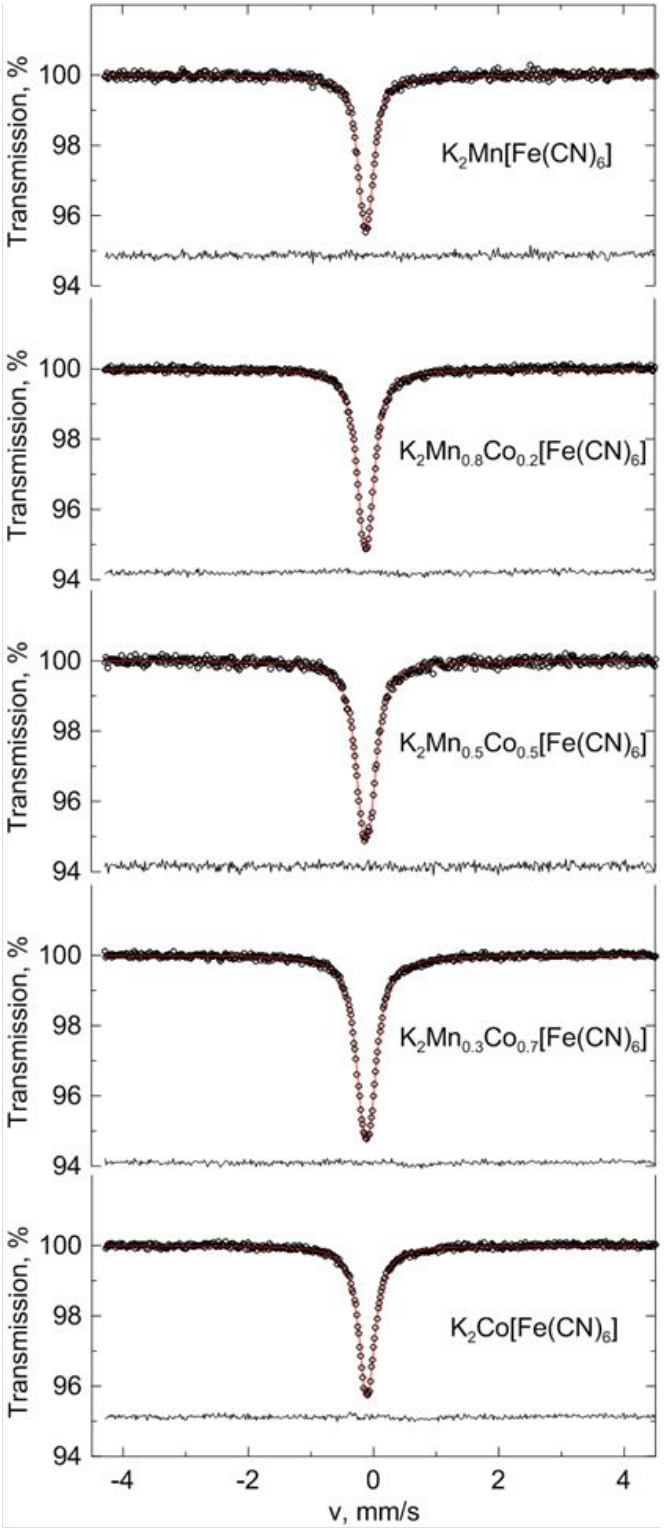

Figure S11. The ^{57}Fe Mössbauer spectra of $K_{2-\delta}Co_xMn_{1-x}[Fe(CN)_6]$ with x=0, 0.2, 0.5, 0.6, 1.0 in ±4.5 mm/s velocity

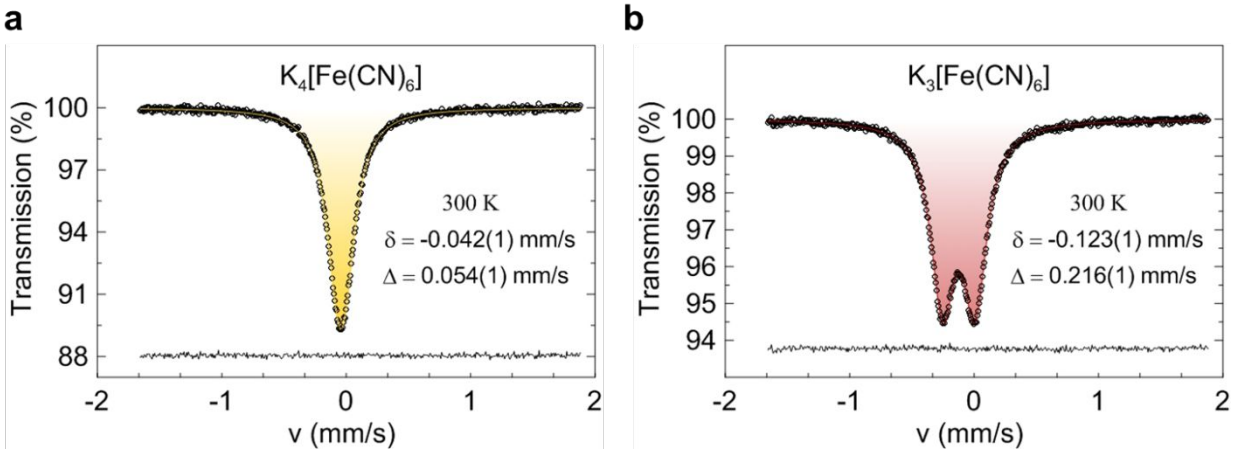

Figure S12. The Mössbauer spectra of (a) $K_4[Fe^{II}(CN)_6]\cdot 3H_2O$, and (b) $K_3[Fe^{III}(CN)_6]$.

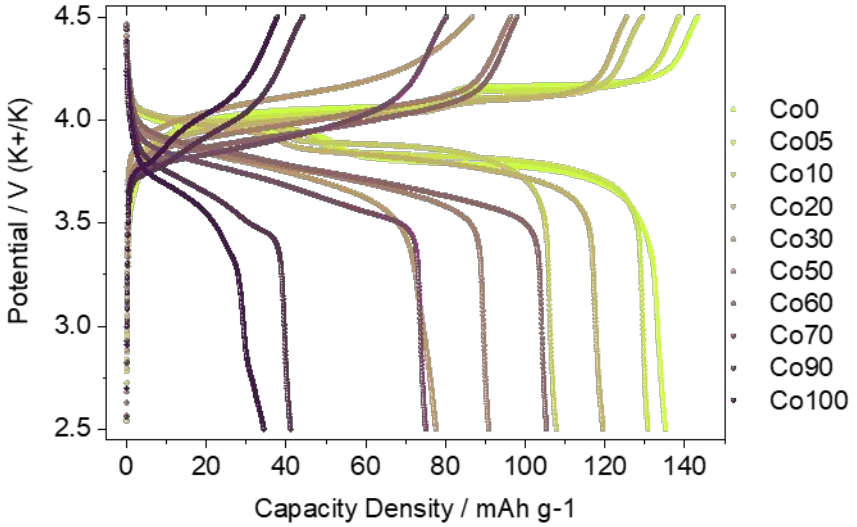

Figure S13. The galvanostatic profiles of 2nd cycles in in the $K_{2-\delta}Co_xMn_{1-x}[Fe(CN)_6]_{1-\gamma}\cdot nH_2O$ (x=0, 0.05, 0.10, 0.20, 0.30, 0.50, 0.60, 0.70, 0.90, 1.00) half-cells, 15 mA g^{-1} current density

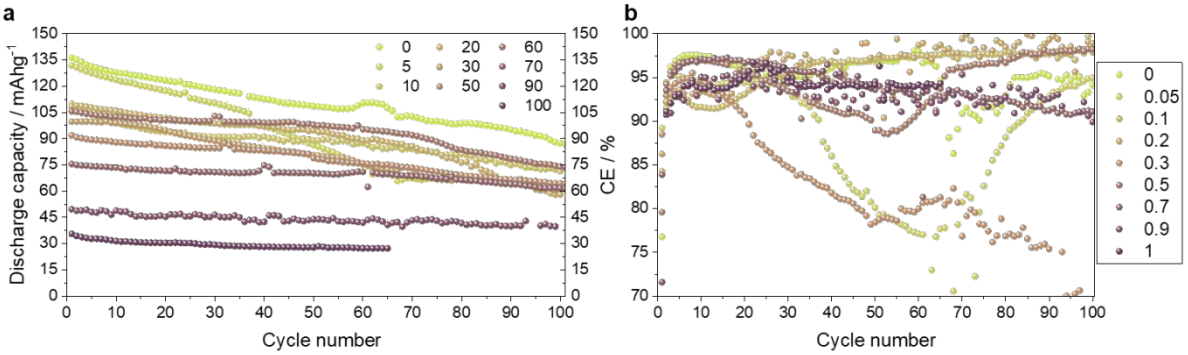

Figure S14. (a) The discharge capacities of the series depending on the cycle number, and (b) coulombic efficiencies of the galvanostatic profiles in the $K_{2-\delta}Co_xMn_{1-x}[Fe(CN)_6]_{1-\gamma}\cdot nH_2O$ (x=0, 0.05, 0.10, 0.20, 0.30, 0.50, 0.60, 0.70, 0.90, 1.00) half-cells, 15 mA g^{-1} current density

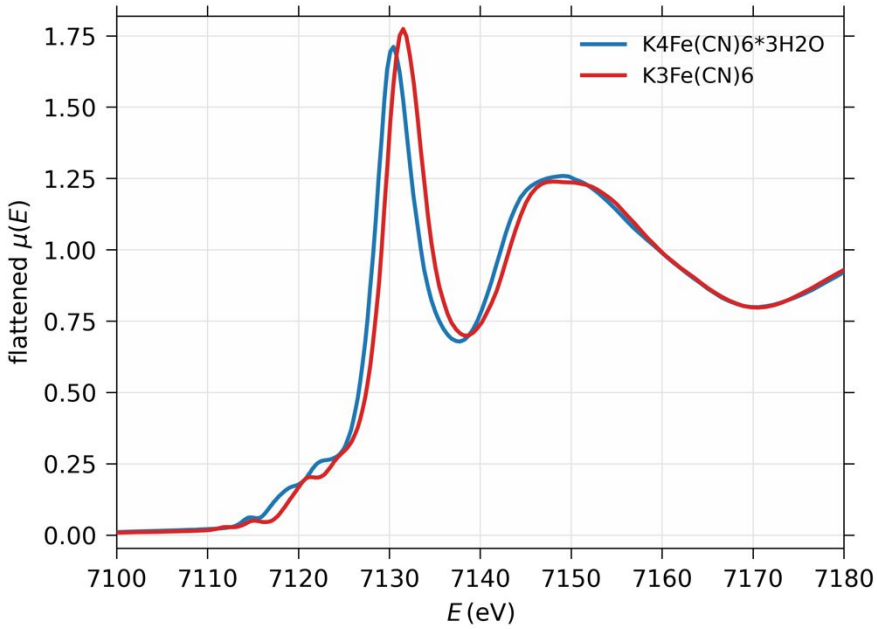

Figure S15. Fe K-edge XANES spectra of the $K_4Fe(CN)_6 \cdot 3H_2O$ and $K_3Fe(CN)_6$ reference materials.

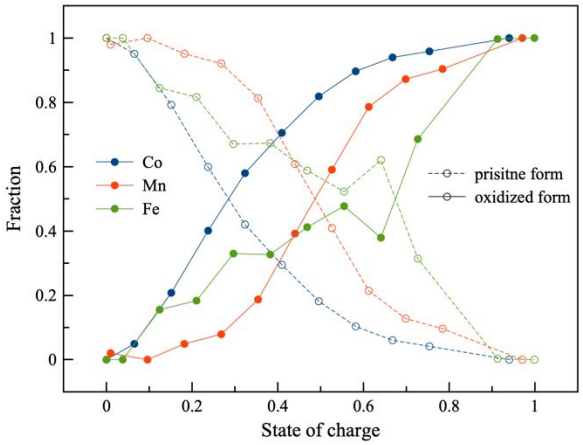

Figure S16. The result of linear combination fit of operando XANES spectra measured at K-edges of Co, Mn, and Fe upon the electrochemical depotassiation of KCMF50 cathode material. Any given spectrum was fitted as the linear combination of the two spectra (the ones of pristine and fully-charged, i.e. oxidized, material at corresponding K-edge) with the restriction fraction(pristine) + fraction(oxidized) = 1.0. The extracted profile for Fe is noisy due to only slight changes in XANES spectra at Fe K-edge were observed (see text for details).

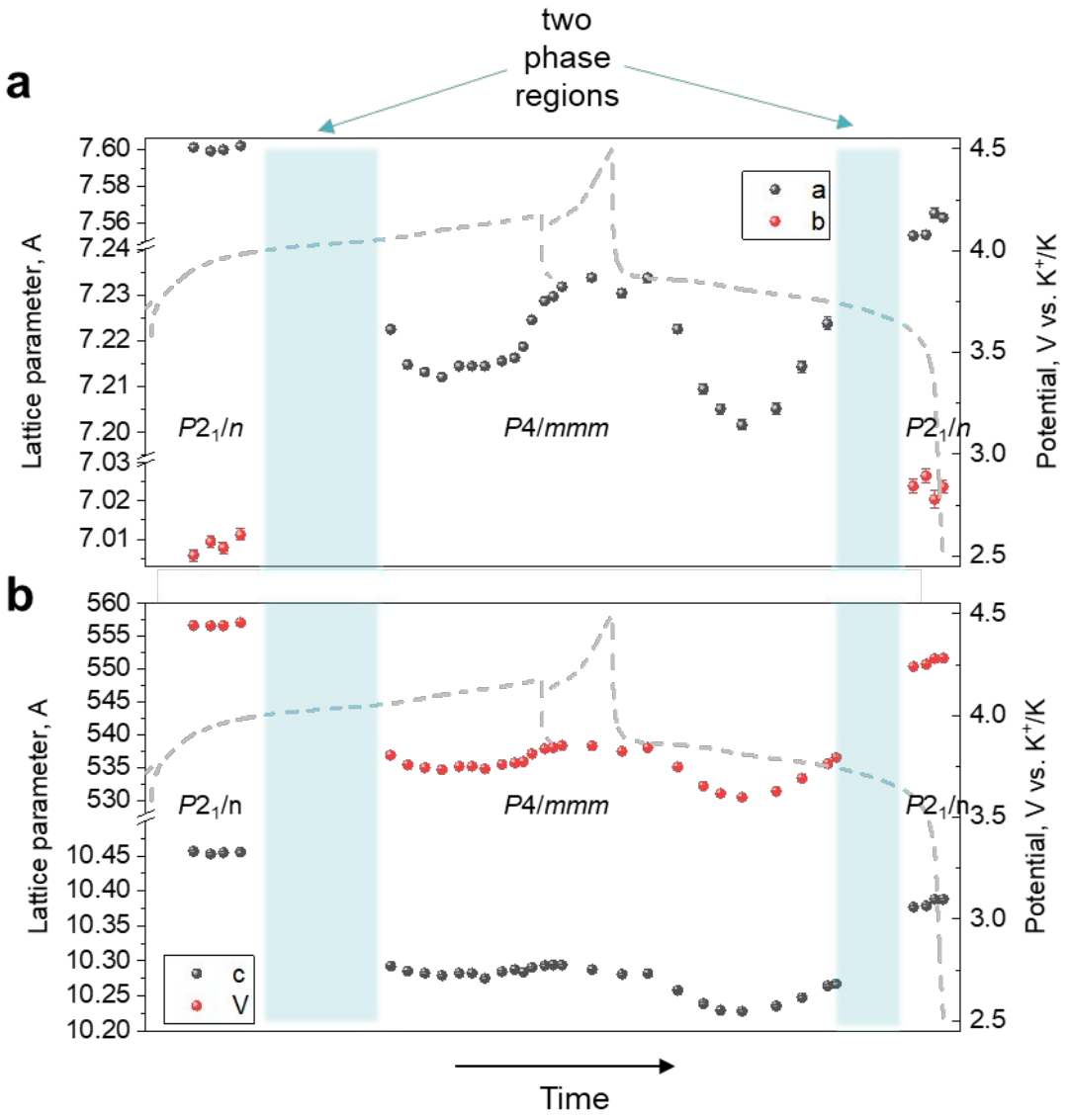

Figure S17. The lattice parameters changes of KCMF50 during *operando* XRD combined with galvanostatic cycling (a) *a* and *b*, (b) *c* and *V*.

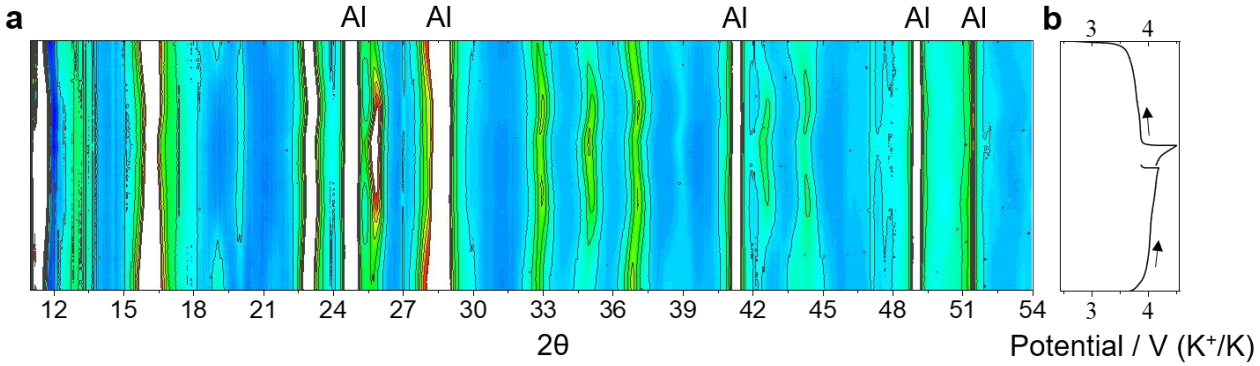

Figure S18. *Operando* (a) S-XRD of KCMF50 and (b) galvanostatic profile of the experiment. Al peaks are at 24.7, 28.5, 41.2, 49.2, 51.6 2θ angles ("White" peaks have too high intensities in the used mask).

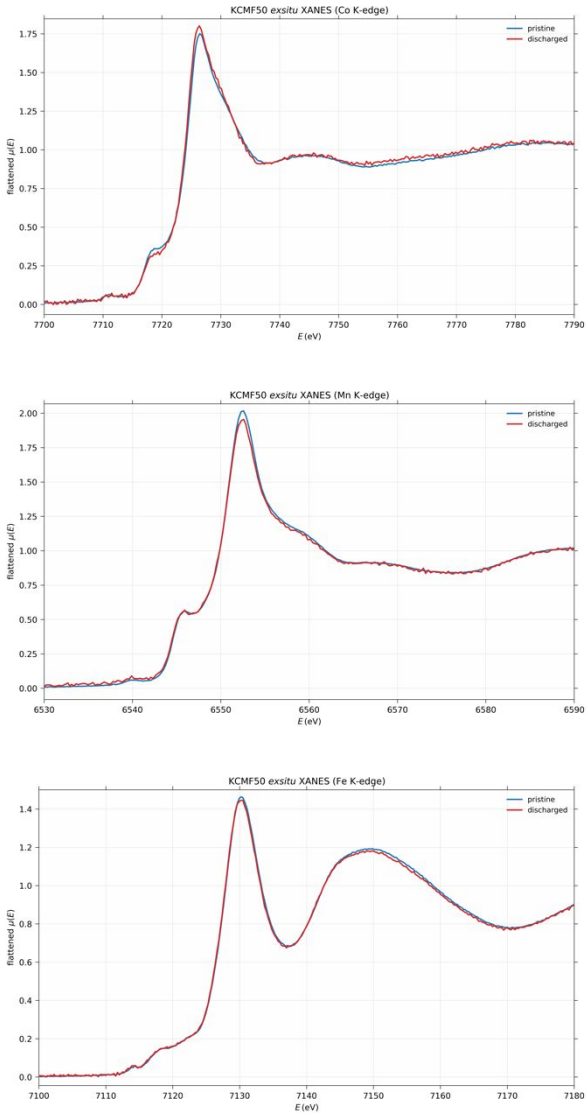

Figure S19. *Ex situ* XANES spectra (cobalt, manganese, and iron K-edges) of the pristine and cycled (charge-dicharge) KCMF50 cathodes.

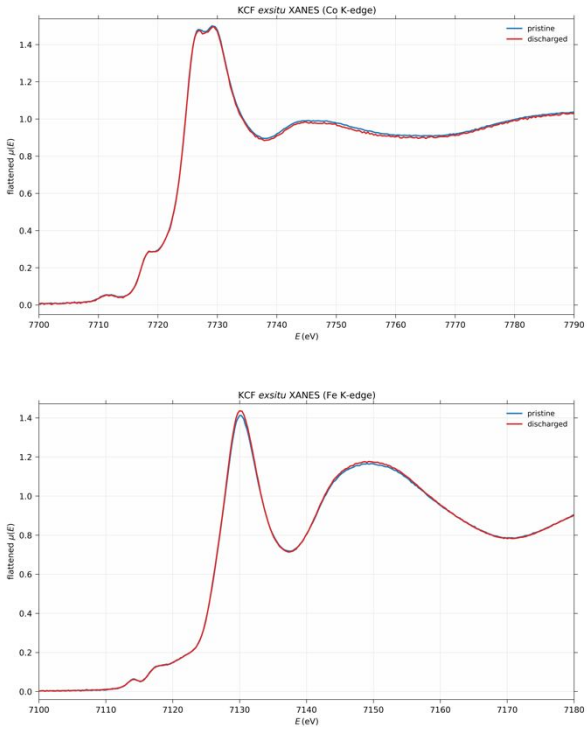

Figure S20. *Ex situ* XANES spectra (cobalt and iron K-edges) of the pristine and cycled (charge-dicharge) KCF cathodes.

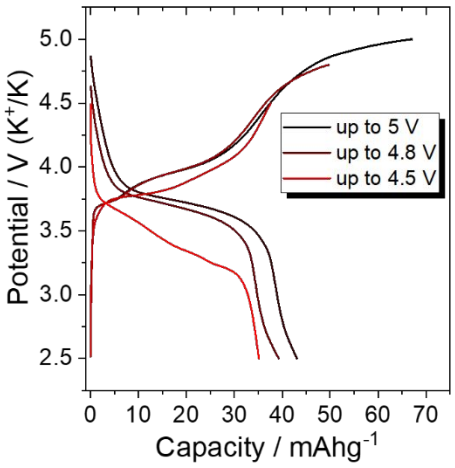

Figure S21. Second cycles of galvanostatic profiles in KCF, where upper potentials differ as 4.5 V (red), 4.8 V (brown), and 5 V (black)

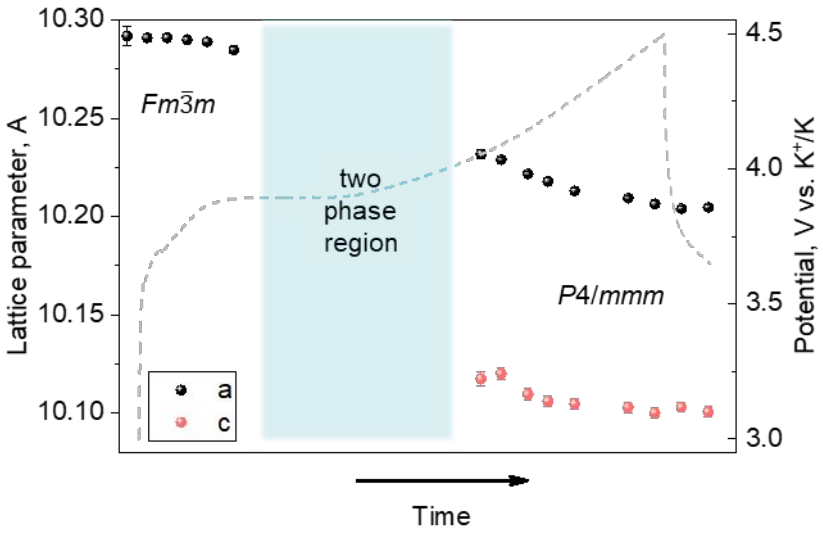

Figure S22. The lattice parameters changes of KCF during *operando* XRD combined with galvanostatic cycling

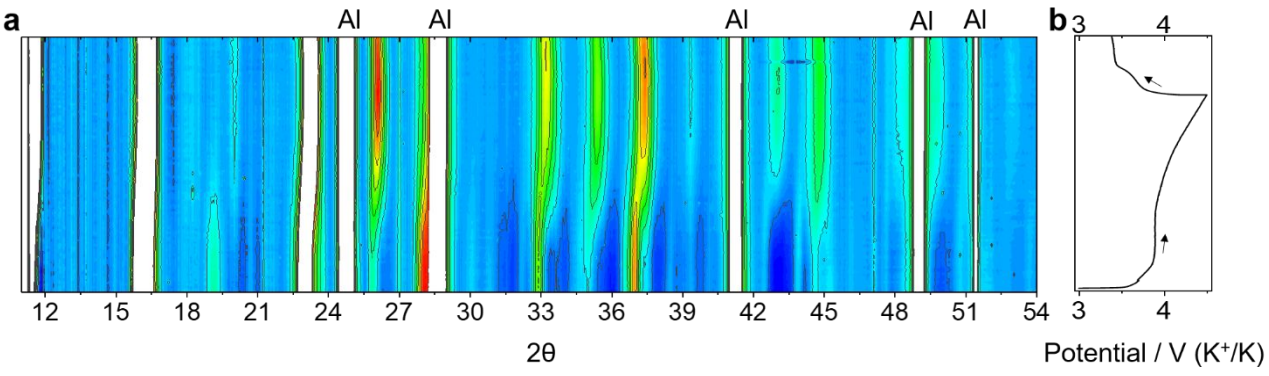

Figure S23. (a) *Operando* S-XRD data of KCF and (b) galvanostatic profile of the experiment. Al peaks are at 24.7, 28.5, 41.2, 49.2, 51.6 2θ angles ("White" peaks have too high intensities in the used mask)